AMERICAN SOCIETY FOR MICROBIOLOGY | Antimicrobial Agents and Chemotherapy®

MECHANISMS OF ACTION: PHYSIOLOGICAL EFFECTS

Chemokine CCL28 Is a Potent Therapeutic Agent for Oropharyngeal Candidiasis

Jie He,[a] Monica A. Thomas,[b] Jaime de Anda,[c] Michelle W. Lee,[c] Emma Van Why,[a] Pippa Simpson,[d] Gerard C. L. Wong,[c] Mitchell H. Grayson,[e,f] Brian F. Volkman,[b] Anna R. Huppler[a]

[a]Department of Pediatrics, Division of Infectious Disease, Medical College of Wisconsin, Milwaukee, Wisconsin, USA
[b]Department of Biochemistry, Medical College of Wisconsin, Milwaukee, Wisconsin, USA
[c]Department of Bioengineering, University of California, Los Angeles, Los Angeles, California, USA
[d]Department of Pediatrics, Division of Quantitative Health Sciences, Medical College of Wisconsin, Milwaukee, Wisconsin, USA
[e]Department of Pediatrics, Division of Allergy and Immunology, The Ohio State University College of Medicine, Columbus, Ohio, USA
[f]The Abigail Wexner Research Institute, Nationwide Children's Hospital, Columbus, Ohio, USA

ABSTRACT *Candida albicans* is a commensal organism that causes life-threatening or life-altering opportunistic infections. Treatment of *Candida* infections is limited by the paucity of antifungal drug classes. Naturally occurring antimicrobial peptides are promising agents for drug development. CCL28 is a CC chemokine that is abundant in saliva and has *in vitro* antimicrobial activity. In this study, we examine the *in vivo Candida* killing capacity of CCL28 in oropharyngeal candidiasis as well as the spectrum and mechanism of anti-*Candida* activity. In the mouse model of oropharyngeal candidiasis, application of wild-type CCL28 reduces oral fungal burden in severely immunodeficient mice without causing excessive inflammation or altering tissue neutrophil recruitment. CCL28 is effective against multiple clinical strains of *C. albicans*. Polyamine protein transporters are not required for CCL28 anti-*Candida* activity. Both structured and unstructured CCL28 proteins show rapid and sustained fungicidal activity that is superior to that of clinical antifungal agents. Application of wild-type CCL28 to *C. albicans* results in membrane disruption as measured by solute movement, enzyme leakage, and induction of negative Gaussian curvature on model membranes. Membrane disruption is reduced in CCL28 lacking the functional C-terminal tail. Our results strongly suggest that CCL28 can exert antifungal activity in part via membrane permeation and has potential for development as an anti-*Candida* therapeutic agent without inflammatory side effects.

KEYWORDS antifungal, antimicrobial peptide, *Candida*, chemokine, oropharyngeal candidiasis

Candidiasis is a serious problem in the care of medically complex patients. Oropharyngeal candidiasis (OPC) afflicts an estimated 10 million people worldwide each year (1). While OPC and other forms of mucosal candidiasis are distinct clinical entities from the high-mortality disseminated disease, mucosal colonization or infection is also a marker of risk for disseminated candidiasis (2–4). Bloodstream infection with *Candida* is the fourth most common nosocomial infection, is rising in incidence in adult intensive care units, and has a 30% to 50% mortality rate (1, 5–7). Control of colonization and invasion in vulnerable patients is necessary to prevent the morbidity and mortality from this pathogen.

Intact immune systems function to exquisitely control colonizing *Candida* and prevent candidiasis (8). With immunodeficiency or barrier dysfunction, antifungal drugs are used to prevent or treat candidiasis. Unfortunately, very limited drug options are approved for use in humans, and all are restricted by cost, drug-drug interactions, and

Citation He J, Thomas MA, de Anda J, Lee MW, Van Why E, Simpson P, Wong GCL, Grayson MH, Volkman BF, Huppler AR. 2020. Chemokine CCL28 is a potent therapeutic agent for oropharyngeal candidiasis. Antimicrob Agents Chemother 64:e00210-20. https://doi.org/10.1128/AAC.00210-20.

Address correspondence to Anna R. Huppler, ahuppler@mcw.edu.

Received 13 March 2020
Returned for modification 21 April 2020
Accepted 15 May 2020
Accepted manuscript posted online 18 May 2020
Published 22 July 2020

adverse effects (1, 9). Information on protective immune responses to *Candida* informs efforts to develop new treatment modalities.

Two incompletely understood molecular components of the immune response to OPC are chemokines and antimicrobial peptides (AMPs). Classic chemokine function is to drive cell migration through gradient formation. AMPs are small peptides with direct antimicrobial properties, including S100 alarmins, β-defensins (BDs), and histatins (Hsts) in the oral cavity. Initially, AMPs and chemokines were ascribed different functions, but studies have shown considerable overlap (10). CCL28 is a CC chemokine with chemotactic activity for leukocytes, *in vitro* AMP activity, and mucosal localization and is a candidate for development as an anti-*Candida* therapeutic.

CCL28 (also known as mucosa-associated epithelial chemokine [MEC]) is a component of the mucosal immune system. It is highly expressed in salivary glands (parotid, submandibular, and sublingual) and modestly expressed in trachea, colon, rectum, mammary gland, and whole tongue (11–14). It has chemotactic activity for lymphocyte subsets (including IgA-secreting plasma cells, T helper 2 [Th2] cells, and T regulatory [Treg] cells) through CCR10 and for eosinophils through CCR3 (12, 15, 16). CCL28 has also been shown to have potent antimicrobial activity against several pathogens *in vitro*, including fungi (*Candida albicans*), Gram-positive bacteria (*Staphylococcus aureus*, *Streptococcus mutans*, and *Streptococcus pyogenes*), Gram-negative bacteria (*Pseudomonas aeruginosa*, *Klebsiella pneumonia*, *Escherichia coli*, and *Salmonella* species), oral anaerobes (*Porphyromonas gingivalis* and *Actinobacillus actinomycetemcomitans*), and parasites (*Leishmania mexicana*) (14, 17–21). We recently confirmed the anti-*Candida* activity of CCL28, which requires the highly charged C-terminal tail but not intact tertiary structure (22). In contrast, tertiary structure is required for receptor-mediated chemotaxis, supporting a distinct attribution of structural motifs to different CCL28 functions (22, 23). When measured, low levels of CCL28 have been reported in humans and mice susceptible to OPC (11, 24). CCL28 is absent in the saliva of patients with primary Sjögren's syndrome, a condition associated with 74% to 87% prevalence of oral candidiasis (24–26). In mice, decreased oral *Ccl28* expression is reported in OPC-susceptible interleukin 17A (IL-17A)-deficient animals (11). However, very little is known about the functional activity of CCL28 in the oral cavity.

The aims of this study were to examine the efficacy of CCL28 against candidiasis *in vivo*, explore the spectrum of anti-*Candida* activity, and elucidate the antimicrobial mechanism. We describe *in vivo* activity of CCL28 against oropharyngeal candidiasis and broad coverage against *C. albicans* strains. CCL28 has extremely rapid activity that disrupts *Candida* membranes. This study provides new information on the activity of CCL28 in infection models and mechanisms that can be exploited for future drug development.

RESULTS

Assessment of *in vitro* potency of wild type CCL28. We previously reported on the relationship between anti-*Candida* properties and structural features of CCL28 (22). The protein used for that study was the UniProt-reviewed 108-amino-acid sequence beginning with Ser-Glu-Ala (SEA) (UniProt identifier [ID] Q9NRJ3) (27). A protein lacking the first 3 amino acids (Δ3-CCL28, UniProt ID A0N0Q3) is predicted to be wild-type CCL28 by several modeling programs (SignalP-5.0, Phobius) and marketed by several commercial vendors (see Fig. S1A in the supplemental material). We first compared the anti-*Candida* activity of SEA-CCL28 against Δ3-CCL28 *in vitro* and found identical dose response curves (Fig. S1B). Similar to that in our previous results, Δ3-CCL28 lacking the C-terminal tail (Δ3-CCL28-Δ80) had reduced anti-*Candida* potency but slightly more activity than the related chemokine, CCL27 (Fig. S1C). Unfolded Δ3-CCL28 (uΔ3-CCL28) is indistinguishable from unfolded SEA-CCL28 (uSEA-CCL28) (Fig. S1D). Based on these results and the predictions for wild-type CCL28, the remainder of the studies were performed using variants of Δ3-CCL28.

Evaluation of CCL28 treatment in candidiasis. Although the potency of CCL28 against *C. albicans in vitro* has been well documented, CCL28 had not previously been

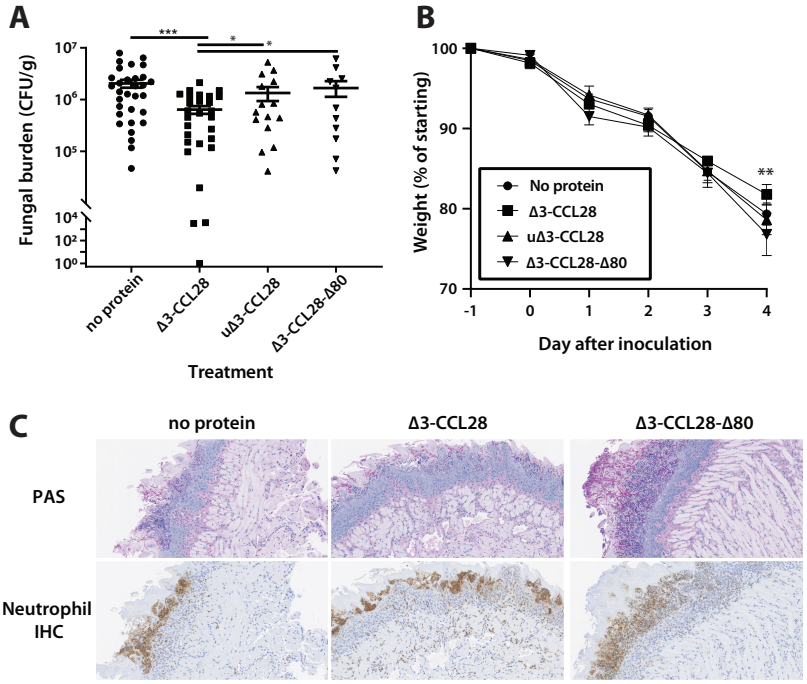

FIG 1 Wild-type CCL28 treatment reduces fungal burden in oropharyngeal candidiasis in highly immunosuppressed mice without excess inflammation. (A and B) High-dose-steroid-treated mice were inoculated orally with *C. albicans* strain CAF2-1 on day 0, followed by once daily topical treatment with variants of human CCL28 in a bioadhesive gel. Tongue fungal burden was measured on day 4 (A) and weight change was recorded daily (B). Means and standard errors of the means (SEMs) are shown. Data are pooled from 5 experiments. In panel B, final weights were significantly different between Δ3-CCL28 and Δ3-CCL28-Δ80 treatments. (C) Representative tongues from OPC-infected mice treated with no protein, Δ3-CCL28, or Δ3-CCL28-Δ80 were examined by periodic acid-Schiff (PAS) staining or immunohistochemistry (IHC) for neutrophils. *, $P < 0.05$; **, $P < 0.01$; ***, $P < 0.001$.

assessed in an animal model of infection (14, 22). The mouse model for OPC faithfully represents human infection and is amenable to topical therapy. OPC was induced in severely immunosuppressed, steroid-treated wild-type mice by using established procedures (28, 29). Delivery of recombinant protein to the oral cavity required a delivery system that did not interfere with *Candida* killing properties. Hydroxypropyl methylcellulose K100 Premium LV bioadhesive gel was selected based on FDA approval for oral consumption and literature on use for oral drug delivery (30–32). Starting 1 day after inoculation with *C. albicans*, the mouse oral cavity was treated with variants of CCL28 or no protein controls in the gel for 60 min daily for 3 days. Variants with known potency based on *in vitro* results were tested: Δ3-CCL28 and uΔ3-CCL28 with high potency and Δ3-CCL28-Δ80 with low potency (Fig. S1B, C, and D) (22). Mice treated with Δ3-CCL28 had a statistically significant decrease in tongue fungal burden on day 4 (0.5 log) (Fig. 1A). As expected, treatment with the lower potency variant Δ3-CCL28-Δ80 did not reduce the tongue fungal burden. Unexpectedly, treatment with high-potency uΔ3-CCL28 also did not result in reduced fungal burdens. Reduced heparin binding resulting in decreased tissue exposure may contribute to the poor efficacy of uΔ3-CCL28 (see Fig. S2). Δ3-CCL28 did not increase oral pain and inflammation as measured by weight loss. Δ3-CCL28-treated mice actually had less weight loss than no-protein-treated mice on day 4 after inoculation, which was more pronounced in male than in female mice (Fig. 1B and Fig. S3). Since CCL28 also has chemotactic properties, the tissue infiltration of *Candida*-fighting neutrophils in fungal plaques was assessed by immunohistochemistry. There was no qualitative difference in neutrophil influx in mice treated with Δ3-CCL28 compared to no protein or Δ3-CCL28-Δ80 treatments (Fig. 1C).

Mice with selective defects in the IL-17 pathway (such as *Il23p19*$^{-/-}$ and *Il17ra*$^{-/-}$ mice) are susceptible to OPC (33). These mice are more moderately immunosuppressed

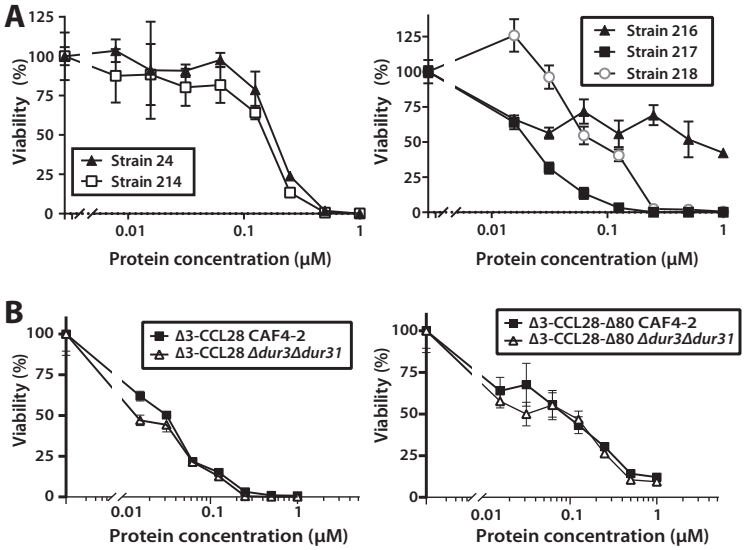

FIG 2 Anti-*Candida* activity of CCL28 is preserved across a range of clinical *C. albicans* strains but not dependent on protein transport. (A) Strains of *C. albicans* isolated from patients with oropharyngeal candidiasis at a final concentration of 2.5×10^4 CFU/ml were incubated with Δ3-CCL28 at a range of concentrations for 2 h. Viability was compared to *C. albicans* treated with buffer without protein. (B) A strain of *C. albicans* lacking two polyamine protein transporters (Δ*dur3* Δ*dur31)* or the parental strain (CAF4-2) was incubated with Δ3-CCL28 or Δ3-CCL28-Δ80 at range of concentrations for 2 h. Viability was compared to that of *C. albicans* treated with buffer. Means and standard deviations (SDs) are shown.

and are models for the human disease chronic mucocutaneous candidiasis (34). Treatment with folded or unfolded CCL28 did not result in decreased oral fungal burdens when OPC was induced in mice with defects in the IL-17 pathway (see Fig. S4). Thus, Δ3-CCL28 treats OPC without detrimental signs of inflammation in highly immunosuppressed mice but not in moderately immunosuppressed mice.

Characterization of anti-*Candida* spectrum. Our work *in vitro* and *in vivo* with CCL28 and its variants generally uses a laboratory strain of *C. albicans* (CAF2-1). To explore the range of activity, we tested the potency of Δ3-CCL28 against 5 clinical strains of *C. albicans*. In 4 of 5 strains, Δ3-CCL28 caused complete or near complete loss of fungal viability at 0.5 μM (50% inhibitory concentration [IC_{50}], 0.021 to 0.186 μM) (Fig. 2A). One strain (strain 216) maintained viability after a 2-h incubation with Δ3-CCL28 (IC_{50}, 1.269 μM) (Fig. 2A). Given this surprising result, we confirmed the species identification of strain 216 as *C. albicans* by matrix-assisted laser desorption ionization–time of flight (MALDI-TOF) mass spectrometry (data not shown) (35). Therefore, Δ3-CCL28 has variable killing potency against different *Candida* strains.

Laboratory strains of *C. albicans* can also be used to probe antimicrobial mechanisms. Strains of *C. albicans* lacking polyamine protein transporters are reported to be relatively resistant to killing by the antifungal peptide histatin 5 (Hst-5) (36). Since the CCL28 C-terminal tail has high homology with Hst-5, we investigated the role of polyamine protein transporters in CCL28 activity (14). Surprisingly, absence of two transporters (*dur3* and *dur31*) did not affect Δ3-CCL28 anti-*Candida* potency (Fig. 2B). This result suggests that CCL28 either uses other protein transporters or does not require any active transport for antimicrobial activity.

Kinetics of CCL28 anti-*Candida* activity. To indirectly assess the requirement for active transmembrane transport of CCL28, we assessed the kinetics of the killing activity. Δ3-CCL28 killed *C. albicans* rapidly, with activity seen as soon as 1 min and 90% loss of viability by 10 min (Fig. 3A). The unfolded protein had even faster activity, with 84% killing by 1 min and complete killing by 4 min (Fig. 3A). In contrast, the clinical antifungal amphotericin B at 4 mg/ml did not affect *C. albicans* viability at 60 min but required 120 min to achieve 80% killing (Fig. 3A and data not shown). We next measured whether CCL28 killing saturates with increasing concentrations of *C. albicans*.

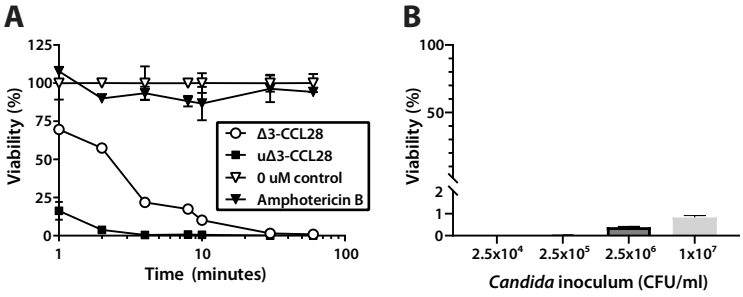

FIG 3 CCL28 treatment results in rapid candidacidal activity and does not saturate with high *Candida* concentrations. (A) The time course of yeast killing was examined by mixing Δ3-CCL28 or uΔ3-CCL28 at a final concentration of 1 μM with *C. albicans* strain CAF2-1 at 2.5×10^4 CFU/ml. Viability was compared to that with no protein buffer or amphotericin B at 4 mg/ml at the same time points. (B) *C. albicans* strain CAF2-1 at a range of concentrations was incubated with Δ3-CCL28 0.5 μM, and viability was determined after 2 h. Means and SDs are shown.

In the range of 2.5×10^4 CFU/ml (the concentration used for killing assays) and 1×10^7 CFU/ml, no real decline in potency was observed (Fig. 3B). Thus, CCL28 rapidly kills *C. albicans* without signs of consumption in yeast cultures at densities ranging up to 7 orders of magnitude.

Membrane disruption by CCL28. To further investigate the role of protein transporters or other active *Candida* cellular processes in CCL28 antimicrobial activity, we examined membrane disruption in paraformaldehyde (PFA)-killed yeast. *C. albicans* yeast was rendered nonviable by a 30-min treatment with PFA. Yeast were then treated with low-salt potassium phosphate buffer (PPB), Δ3-CCL28, or Δ3-CCL28-Δ80 for 10 min. Propidium iodide (PI) uptake was measured in treated cells by flow cytometry to assess membrane disruption. PFA-killed yeasts treated with PPB had rare uptake of PI, while CCL28 treatment resulted in high levels of PI uptake (Fig. 4A). A higher percentage of Δ3-CCL28-treated cells than Δ3-CCL28-Δ80-treated cells were PI^+ under the same conditions (Fig. 4B). Treatment of live *C. albicans* yeast with PPB, PFA, or Δ3-CCL28 revealed similar patterns, with minimal membrane disruption by PFA but close to 100% PI^+ cells with 10 min of Δ3-CCL28 treatment (Fig. 4C). Since Δ3-CCL28 and Δ3-CCL28-Δ80 have markedly different killing potencies, dose response curves for the two variants were determined using membrane disruption assays (Fig. 4D and E). Treatment with either variant resulted in membrane disruption in almost all cells at high concentrations, but Δ3-CCL28 caused disrupted membranes in more cells than Δ3-CCL28-Δ80 at moderate concentrations. The 50% effective concentration (EC_{50}) for Δ3-CCL28 ranged from 0.07 to 0.071 μM, while the EC_{50} for Δ3-CCL28-Δ80 was 0.158 to 0.0223 μM (data not shown). Membrane disruption for the dose response curves was measured by both PI uptake (Fig. 4D) and intracellular enzyme leakage (adenylate kinase) (Fig. 4E), with similar patterns. Thus, Δ3-CCL28 treatment causes rapid membrane disruption in *Candida* without a requirement for active cellular processes.

Induction of negative Gaussian curvature in membranes by CCL28. To characterize the peptide-membrane interaction mediated by CCL28, we used small-angle X-ray scattering (SAXS) to test the membrane remodeling capacity of CCL28 on small unilamellar vesicles (SUVs). Specifically, we used SAXS to assess whether negative Gaussian curvature (NGC), the type of curvature topologically required for membrane permeation mechanisms such as pore formation, blebbing, and budding, can be induced in a target membrane. This method has been used extensively to characterize the interaction of curvature-inducing peptides and proteins with prokaryotic and eukaryotic membranes (37–42). To assess the ability of CCL28 to remodel yeast and mammalian membranes, we tested whether CCL28 has the capacity to induce negative Gaussian curvature necessary for membrane permeation and, if so, what amount of NGC is produced by the interaction of Δ3-CCL28 with SUVs of two different membrane compositions: one mimicking *Candida* membranes and another modeling mammalian

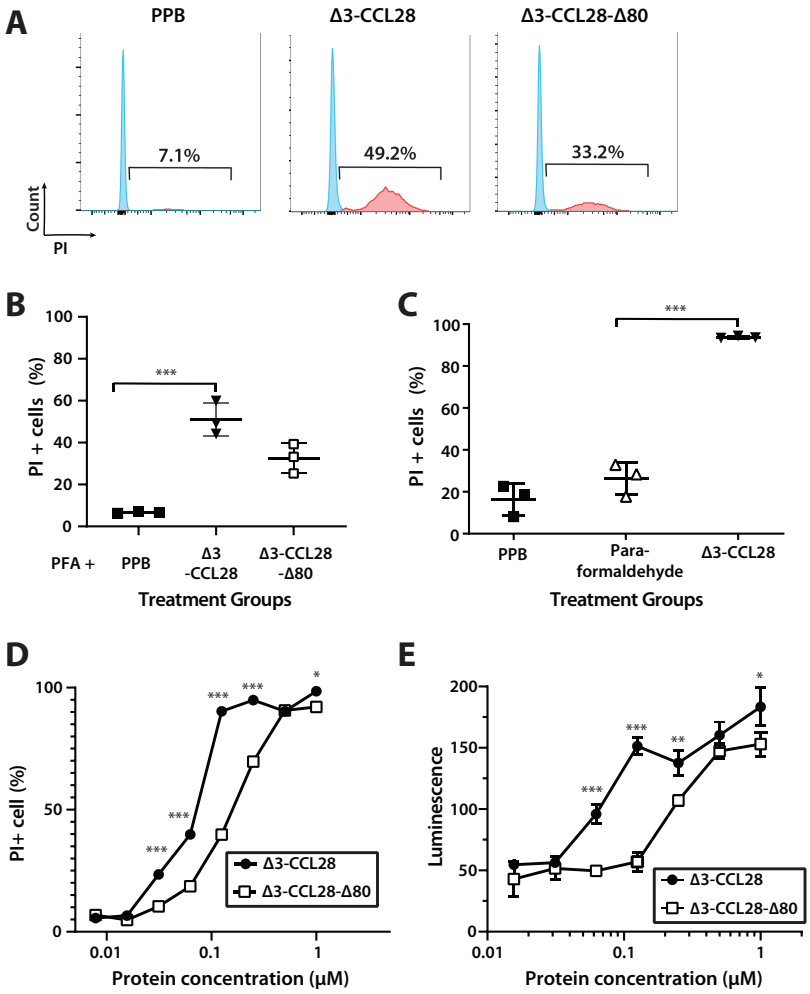

FIG 4 CCL28 disrupts *Candida* membranes independent of active cell metabolism in a dose-dependent manner. (A and B) *C. albicans* at a final concentration of 2.5×10^6 CFU/ml was chemically killed with paraformaldehyde for 30 min, followed by treatment with potassium phosphate buffer (PPB) or the indicated CCL28 variant at 0.25 μM for 10 min. Membrane disruption was measured by propidium iodide (PI) uptake and quantified with flow cytometry. (A) Representative histograms of mean fluorescence intensity for PI. (B) Aggregate data representing two experiments. (C) Live *C. albicans* was treated with PPB, paraformaldehyde, or 0.25 μM Δ3-CCL28 for 10 min. The percentage of *Candida* with uptake of PI was measured by flow cytometry. (D) Dose response curves for PI uptake measured by flow cytometry were determined for *C. albicans* treated with Δ3-CCL28 or Δ3-CCL28-Δ80. (E) Dose response curves for adenylate kinase leakage measured by luminescence were determined for *C. albicans* treated with Δ3-CCL28 or Δ3-CCL28-Δ80. Means and SDs are shown. *, $P < 0.05$; **, $P < 0.01$; ***, $P < 0.001$.

cells. The *Candida* membranes were modeled with a lipid composition of 1,2-dioleoyl-*sn*-glycero-3-phospho-L-serine/1,2-dioleoyl-*sn*-glycero-3-phosphoethanolamine at a molar ratio of 20/80 (DOPS/DOPE 20/80). To model mammalian membranes, we incorporated 1,2-dioleoyl-*sn*-glycero-3-phosphocholine (DOPC) to obtain a lipid molar ratio of DOPS/DOPE/DOPC 20/40/40. The SUV suspensions were incubated with Δ3-CCL28 at protein-to-lipid (P/L) molar ratios 1/80, 1/160, and 1/320 (i.e., P/L charge ratios of 1/1, 1/2, and 1/4, respectively).

Δ3-CCL28 restructured *Candida*, but not mammalian, model membranes into NGC-rich cubic phases. SAXS spectra for the *Candida*-like membranes incubated with Δ3-CCL28 exhibited correlation peaks with Q-ratios of $\sqrt{6} : \sqrt{14} : \sqrt{16} : \sqrt{20} : \sqrt{22}$ (for P/L = 1/80), $\sqrt{2} : \sqrt{3} : \sqrt{4}$ (for P/L = 1/160), and $\sqrt{2} : \sqrt{3}$ (for P/L = 1/320) corresponding to Ia3d, Pn3m, and Pn3m cubic phases with 4.27×10^{-2} nm^{-2}, 1.53×10^{-2} nm^{-2}, and 1.77×10^{-2} nm^{-2} mean NGC per unit cell ($|\langle K \rangle|$), respectively (Fig. 5A). This capacity to remodel membranes was not observed for Δ3-CCL28 with mammalian-like mem-

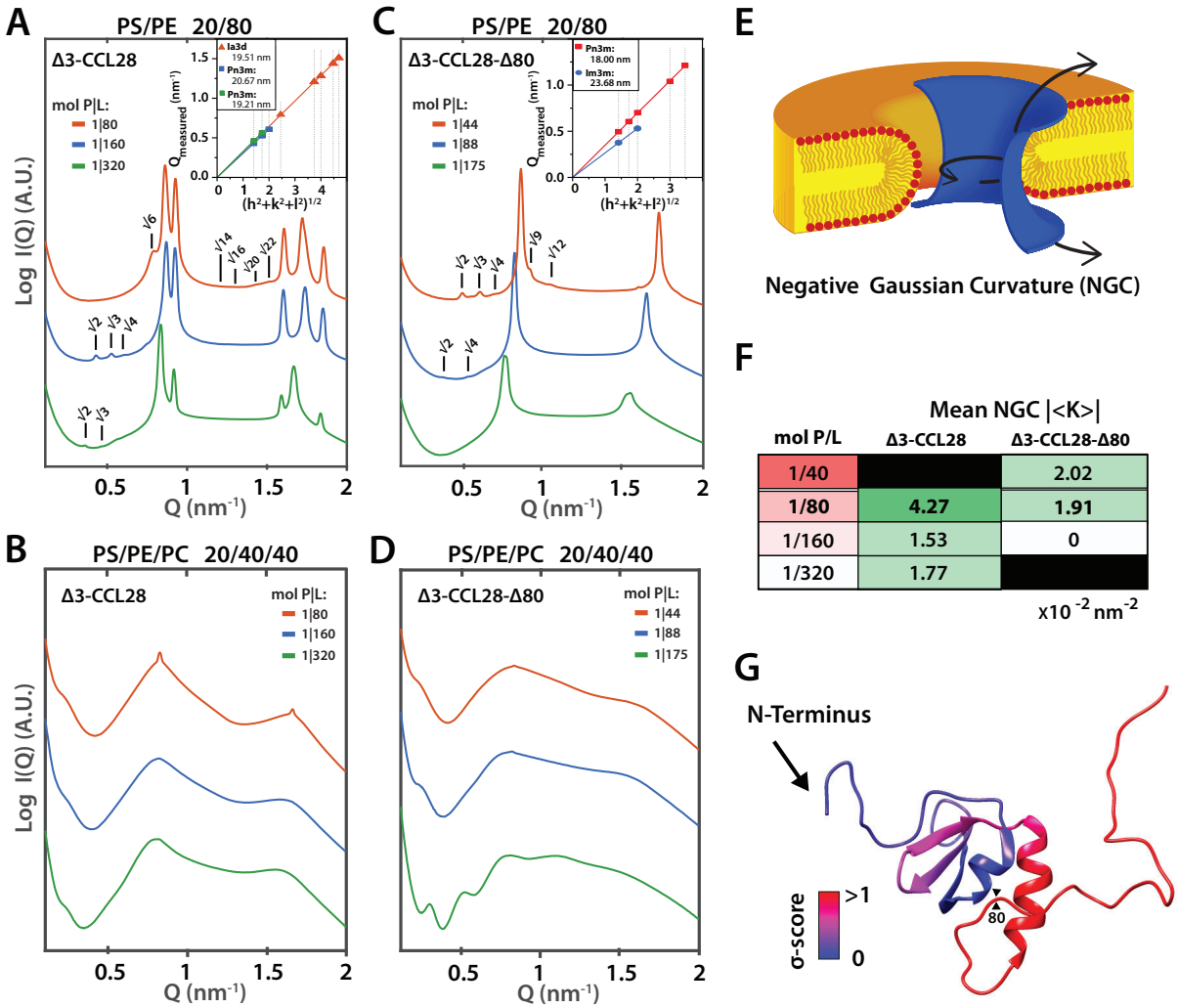

FIG 5 Δ3-CCL28 induces negative Gaussian curvature of *Candida*-like membranes, which is reduced with C-terminal truncation. (A) SAXS spectra indicate that Δ3-CCL28 induces negative Gaussian curvature (NGC) in *Candida*-like model membranes (DOPS/DOPE 20/80) and consequently generates cubic phases. The type of cubic phase thus generated and the cubic lattice parameters calculated from fits to the data are shown in the inset. (To facilitate visualization, spectra have been manually offset in the vertical direction by scaling each trace by a multiplicative factor.) (B) In contrast, SAXS spectra indicate that Δ3-CCL28 does not induce NGC in mammalian model membranes (DOPS/DOPE/DOPC 20/40/40), and no cubic phases are observed. Δ3-CCL28-Δ80 interacts with *Candida*-like (C) and mammalian (D) model membranes. Cubic phases with different lattice constants and therefore different quantitative amounts of NGC are induced for the DOPS/DOPE 20/80 *Candida*-like model membrane, whereas no cubic is observed for the DOPS/DOPE/DOPC 20/40/40 mammalian model membrane. (E) A region of NGC (blue saddle-shaped surface) is highlighted in a schematic transmembrane pore. (F) Table of the calculated mean NGC values induced by Δ3-CCL28 and Δ3-CCL28-Δ80 on *Candida*-like membranes for each P/L molar ratio tested (within a 10% error): note that at the same molar ratio P/L of 1/80, Δ3-CCL28 induces more than 2× the amount of NGC as Δ3-CCL28-Δ80, implying a greater degree of membrane deformation per molecule. (G) σ-scores predicted by a support vector machine (SVM) classifier projected on the 3D crystal structure of CCL28 (RCSB PDB 6CWS). The red parts (higher σ score) of the structure are "hot spots" for NGC generation and have greater propensity to induce NGC in membranes than the blue parts of the structure (lower σ score) (43). These hot spots can be seen in the α-helix and in the C-terminal tail.

branes, which instead exhibit form factors with weak multilamellar ordering at a 1/80 P/L molar ratio (Fig. 5B). In other words, Δ3-CCL28 can induce membrane curvatures that contribute to membrane permeation in our model for *Candida* membranes but not in our model for mammalian membranes.

To understand the contribution of the histidine-rich C-terminal tail of CCL28 to this mechanism of membrane remodeling, we repeated the SUV-peptide interaction experiments with Δ3-CCL28-Δ80 and the model membranes mentioned above, at P/L molar ratios of 1/44, 1/88, and 1/175 (maintaining P/L charge ratios of 1/1, 1/2, and 1/4, respectively). The results recapitulate the Δ3-CCL28 selectivity results. The truncated CCL28 was able to induce NGC in model *Candida*-like membranes but not in

mammalian-like membranes (Fig. 5C and D). The SAXS spectra for the *Candida*-like membranes interacting with Δ3-CCL28-Δ80 show the presence of cubic phases with peaks characterized by Q-ratios of $\sqrt{2} : \sqrt{3} : \sqrt{4} : \sqrt{9} : \sqrt{12}$ (for P/L = 1/44) and $\sqrt{2} : \sqrt{4}$ (for P/L = 1/88), which correspond to Pn3m and Im3m cubic phases with mean NGC $|<K>|$ values of 2.02×10^{-2} nm^{-2} and 1.91×10^{-2} nm^{-2}, respectively. No cubic phases, however, were observed at a P/L molar ratio of 1/175 (Fig. 5C). Interestingly, although Δ3-CCL28-Δ80 was able to induce membrane remodeling, it required a larger number of peptide molecules to induce the same quantitative level of NGC deformation as Δ3-CCL28, which can be seen in the table (Fig. 5F). At a P/L molar ratio of ~1/160, Δ3-CCL28-Δ80 was not able to induce NGC, while Δ3-CCL28 induced a mean NGC $|<K>|$ of 1.53×10^{-2} nm^{-2}. Furthermore, at a P/L molar ratio of ~1/80, Δ3-CCL28 induced more than 2× the quantitative amount of mean NGC per volume than Δ3-CCL28-Δ80, with $|<K>|$ values of 4.27×10^{-2} nm^{-2} and 1.91×10^{-2} nm^{-2}, respectively. That the reduction of membrane remodeling capacity correlates with the absence of the histidine-rich tail in Δ3-CCL28-Δ80 is striking and suggests that the tail contributes to membrane permeation. The contribution of the C-terminal tail to membrane permeabilization is consistent with machine learning predictions. Using a previously validated support vector machine (SVM) classifier trained on α-helical AMP sequences (43), we screened the CCL28 sequence, implementing a variable moving window to produce a composite σ-score assigned to each amino acid (Fig. 5G). We have previously shown that this σ-score output by the SVM classifier correlates with the peptide's ability to generate NGC (43, 44). From this *in silico* screening, we observed that the highest scoring parts of CCL28 are localized at two places, the histidine-rich C-terminal tail and the α-helix common to the chemokine fold. Therefore, the loss of the C-terminal tail is expected to correlate with a partial loss of NGC-inducing function against membranes. Unlike classical AMPs, the existence of two distinct and separated membrane curvature-generating elements in CCL28 may potentiate activity not found in AMPs.

DISCUSSION

AMPs with direct anti-*Candida* activity are a component of the oral mucosal immune system (45, 46). Mimicking the natural immune responses has the potential to open up new classes of antifungal agents (47). This approach requires detailed knowledge of the activity and mechanism of the candidate molecule in order to preserve therapeutic activity while minimizing pathological side effects. For example, IL-17 is a potent mediator of anti-*Candida* immune responses, but oral application in mice results in severe local tissue inflammation precluding its use as a therapy (33). In the present study, we describe the activity of CCL28 against oral candidiasis and several strains of *Candida* as well as the mechanism of action.

We demonstrate that wild-type CCL28 reduces fungal burdens in a model of OPC (Fig. 1) (30, 48). Interestingly, efficacy was only seen in highly immunosuppressed steroid-treated mice. More moderately immunosuppressed mice with genetic defects in the IL-17 pathway had no change in oral fungal burden with CCL28 treatment (see Fig. S4 in the supplemental material). This may be due to differences in oral cavity conditions in mice with different immune defects. CCL28 activity is known to be highly sensitive to salt and pH (14, 22). In addition, CCL28 is susceptible to degradation by salivary proteolytic enzymes, which can have variable compositions. It is likely that enhanced susceptibility to degradation contributed to the lack of efficacy of unfolded CCL28 in the oral cavity. Exogenous CCL28 treatment may have higher efficacy in cases of salivary CCL28 deficiency, such as Sjögren's syndrome (24). CCL28 at concentrations physiologically present in healthy human saliva (30 to 63 nM in whole saliva and 65 to 232 nM in parotid secretions) is active against *C. albicans in vitro* (14, 22). Recently described mouse models of CCL28 deficiency will allow for future study of the role of endogenous CCL28 in the oral cavity (49, 50).

The activity of CCL28 against *Candida* strains is not universal. CCL28 was highly potent against several clinically derived strains of *C. albicans* (Fig. 2). Further study of the strain resistant to CCL28 may reveal new insights into *Candida* biology or CCL28

mechanisms. The mechanism of action of many clinically available antifungal agents, including azoles and polyenes, involves the *Candida* membrane (51). These drugs inhibit synthesis or bind to membrane sterols. The membrane-disrupting activity of CCL28 may be additive or synergistic with membrane-active antifungal agents. Synergy would be especially useful in treating drug-resistant species, such as *Candida glabrata*. We noted that amphotericin B, a clinically approved polyene, acts very slowly to kill *C. albicans*. An additional advantage to CCL28 in the treatment of candidiasis is the rapid activity without saturation with high *Candida* loads (Fig. 3).

The intriguing AMP activity of CCL28 was first investigated due to the homology of the C terminus with Hst-5 (14, 52). Hst-5 is a well-described anti-*Candida* peptide that requires an intact C-terminal domain and α-helical conformation for activity (52). Unlike many AMPs that appear to kill through membrane disruption, the anti-*Candida* activity of Hst-5 requires intracellular localization (53). In mice, promising work on Hst-5 engineered for prolonged stability showed a therapeutic effect in OPC (54). In the case of CCL28, the importance of the C-terminal tail was confirmed by studies of C-terminal truncation mutants of CCL28 against bacterial species and our own work with *C. albicans* (22, 55). The mechanism of CCL28 anti-*Candida* activity was previously incompletely explored, but early studies of full-length CCL28 pointed toward a mechanism distinct from that of Hst-5 (14).

Our work reveals that the mechanism of antimicrobial activity of CCL28 is rapid membrane disruption. Although the end effect of Hst-5 exposure is *Candida* cell death and loss of membrane integrity, this is a relatively slow process, starting after 10 min and requiring 90 min for complete killing (45). In contrast, >80% of *C. albicans* cells are nonviable after less than 10 min of incubation with CCL28 (Fig. 4). The activity of Hst-5 requires active cell transport to an intracellular location (36, 53). CCL28 activity on the cell membrane does not require the same polyamine transporters and in fact does not seem to require any active cellular processes (Fig. 2 and 4). In addition to direct assays of membrane permeation, we demonstrated with SAXS the capacity of CCL28 to induce changes directly in *Candida*-like membranes that are necessary for pore formation and other membrane permeation mechanisms. The induction of NGC also occurred without the contribution of intracellular machinery. Finally, residual anti-*Candida* activity in the C-terminal truncated mutant (SEA-CCL28-Δ80 or Δ3-CCL28-Δ80) and the SVM classifier support that some of CCL28's anti-*Candida* activity resides in the protein core and not just the charged C-terminal tail (Fig. S1) (22). This may explain the differences in mechanism from that of Hst-5.

There is an intriguing association between mucosal localization of chemokines and potent or broad antimicrobial activity (reviewed in reference 56). CCL28 presence or absence at mucosal sites has been linked to alterations in homeostatic or disease conditions associated with microbes. CCL28 is modestly expressed in the gut epithelium, and its absence is reported to alter the fecal microbiome (12, 49). Levels of CCL28 in gingival crevicular fluid are elevated in periodontal disease (57). In addition to high concentrations in saliva, CCL28 is expressed at multiple locations in the mouth, including lingual epithelium (11, 50). Another example of an antimicrobial mucosal chemokine is CXCL17. It is expressed in tongue, respiratory, and colonic mucosa and has broad activity against bacteria and fungi commonly localized to these sites (58). A key role for antimicrobial chemokines is implied by their localization at the site of first defense from pathogens.

This study investigated immune cell-independent CCL28 activity. However, CCL28 is known to be chemotactic for some types of lymphocytes and eosinophils, including IgA-secreting plasma cells (12, 15, 16). Exogenous CCL28 treatment may increase the number of oral mucosal plasma cells and result in changes in salivary IgA levels. However, salivary IgA concentration does not necessarily correlate with protection from oral candidiasis (59, 60). Receptor-mediated chemotactic activity requires intact tertiary structure and likely requires the N terminus based on studies of other chemokines (23, 61, 62). Neutrophils are the key immune cell recruited in response to candidiasis, usually through CXC chemokines (63). Tissue histology after CCL28 treatment did not show

TABLE 1 *Candida* strains

C. albicans strain name	Feature(s)	Reference
CAF2-1	Laboratory strain	67
24	Clinical isolate, oral	NA[a]
214	Clinical isolate, oral	NA
216	Clinical isolate, oral	NA
217	Clinical isolate, oral	NA
218	Clinical isolate, oral	NA
CAF4-2	Laboratory strain, parental strain of the Δ*dur3* Δ*dur31* strain	67
Δ*dur3* Δ*dur31*	DUR3 and DUR31 deficiency	36

[a]NA, not available.

major changes in neutrophil recruitment to fungal plaques (Fig. 1). However, reports of possible CCL28-relevant receptors on neutrophils suggests the possibility of an additional mechanism of neutrophil recruitment (64, 65).

Overall, our findings indicate a role for CCL28 in combatting *Candida* in the oral cavity and its potential for augmenting or accelerating the activity of membrane-active clinical antifungal agents.

MATERIALS AND METHODS

Protein preparation. All studies were performed with variants of human CCL28. SEA-CCL28 (GenScript; UniProt ID Q9NRJ3 [29]), Δ3-CCL28 (UniProt ID A0N0Q3), or truncation variants were cloned, expressed, and purified as previously described (22, 66). High-performance liquid chromatography (HPLC) and linear trap quadrupole (LTQ) mass spectrometry were used to verify protein identity and purity. Unfolded protein was generated through reduction of disulfide bonds with 5 mM dithiothreitol (DTT) in a buffer containing 100 mM NH_4HCO_3 and 6 M urea at pH 7.8. To maintain the reduced bonds, 20 mM iodoacetamide was added to alkylate cysteine residues and incubated for 60 min in the dark at room temperature followed by quenching with 5 mM DTT. The alkylated product was dialyzed with three buffer changes in 100 mM NH_4HCO_3. The solubilized (by pH adjustment) alkylated product was purified by HPLC. The identity of the alkylated product was confirmed by mass spectrometry. Heparin binding capacity was assessed using a 1-ml HiTrap heparin HP column (GE Healthcare Life Sciences, Pittsburgh, PA). Proteins were run with a gradient of 0% to 100% 1 M NaCl, and absorbance was measured on an AKTA start chromatography system (GE Healthcare Life Sciences, Pittsburgh, PA).

***Candida* strains and growth.** Candida strains used in this study are listed in Table 1 (36, 67). Experiments were performed with strain CAF2-1 unless otherwise noted. *Candida* was grown on yeast extract-peptone-dextrose (YPD; Difco, Fisher, Pittsburgh, PA) medium. Growth medium was supplemented with uridine (Millipore Sigma, MO, USA) at a final concentration of 50 μg/ml for growth of uridine-deficient strains (CAF4-2 and Δ*dur3* Δ*dur31*). Stocks were stored at −80°C and streaked on YPD agar plates monthly for routine use. For experiments, *Candida* was cultured from a single colony in 10 ml of YPD medium at 30°C with 250 rpm shaking for 16 to 20 h. Cell concentration was determined on a NanoDrop 2000 spectrophotometer (Thermo Scientific, MA) with and optical density at 600 nm (OD_{600}) of 1.2 to 1.3 corresponding to 2×10^7 CFU/ml. Cells were washed twice with phosphate-buffered saline (PBS), pH 7.4, and resuspended at 2×10^7 CFU/ml in 1× PBS.

Mice. *Il23p19*$^{-/-}$ mice on a C57BL/6 background were provided by Genentech (South San Francisco, CA). *Il17ra*$^{-/-}$ mice on a C57BL/6 background were provided by Amgen (Seattle, WA). All other mice were C57BL/6J mice originally from The Jackson Laboratory (Bar Harbor, ME). Colonies were bred and maintained in-house in a specific-pathogen-free environment. Mice were 6 to 10 weeks old, with both male and female mice included in experimental cohorts. Animal protocols were approved by the Medical College of Wisconsin Institutional Animal Care and Use Committee (IACUC).

Mouse immunosuppression. Select mice were immunosuppressed with high-dose steroid treatment to induce susceptibility to OPC. Kenalog (Henry Schein Medical, Melville, NY) was administered subcutaneously at a dose of 20 μg/g mouse body weight every other day starting on day −1.

OPC mouse model. The mouse model of OPC was performed as previously described (28, 29). In brief, mice were anesthetized with ketamine (Henry Schein Animal Health, Dublin, OH) and xylazine (Henry Schein Animal Health, Dublin, OH), and oral cavities were swabbed to evaluate for preexisting *Candida* colonization. *Candida* strain CAF2-1 at 2×10^7 CFU/ml was soaked into a 2.5-mg cotton ball and placed sublingually for 75 min to inoculate mice. A PBS-soaked cotton ball was used for sham-inoculated mice. Mice were weighed daily starting at day −1. Oral fungal burden was measured in whole-tongue tissue on day 4. Tongues were weighed and homogenized in 1 ml of PBS using a Bullet Blender Storm homogenizer (Midwest Scientific Inc, Valley Park, MO). The tissue suspensions were diluted to 1:20 and 1:200 with PBS, and 50 μl of each dilution was spread in triplicates on YPD plates supplemented with 50 μg/ml kanamycin and 100 μg/ml ampicillin. Plates were incubated at 30°C for 48 h followed by colony counting.

CCL28 oral treatment. CCL28 protein variants were reconstituted to 400 μM in 1 mM potassium phosphate buffer (PPB), aliquoted as 50-μl vials, and stored at −20°C. HPMC K100 premium LV gel

(Colorcon Inc., WI, USA) was dissolved in PPB to make 4% gel, aliquoted into 4-ml vials, and stored at 4°C. On the day of treatment, protein variant stocks or equal volumes of PPB were added to the gel to reach a final concentration of 10 μM variant protein and mixed by inverting the tube 30 times. The protein-gel mixtures were kept on ice until administration. Anesthetized mice were treated in the oral cavity with 50 μl of the protein-gel mixture daily starting on day +1 after *Candida* inoculation. Mouse were maintained sedated and supine for 60 min during treatment.

Histologic analysis of mouse tongues. Tongues were collected on day 2 from the *Candida*-inoculated mice treated with no protein, Δ3-CCL28, or Δ3-CCL28-Δ80. Tongues were fixed with 10% formalin immediately and processed by the Children's Research Institute (CRI) histology core. Adjacent sections were stained with periodic acid-Schiff (PAS) to visualize fungal plaques and immunohistochemistry (IHC) for neutrophils (NIMP-R14; Abcam, Cambridge, MA). Images were recorded at the CRI Imaging Core using a NanoZoomer digital slide scanner (Hamamatsu Photonics, Japan).

***In vitro* Candida killing assays.** *Candida* strains were cultured as described above. The *Candida* culture was washed twice with 1 mM PPB and then diluted to 5×10^4 CFU/ml on ice. CCL28 variants were dissolved in PPB and serially diluted. For dose response curves, protein dilutions or PPB (100 μl) was mixed with *Candida* suspensions (100 μl) in wells of 96-well round-bottom plates in triplicates. Plates were incubated at room temperature and 80 rpm gentle shaking for 2 h. After incubation, 50 μl of the mixture and/or 1:5 dilutions were spread on YPD or YPD plus uridine (for uridine-deficient strains) plates and incubated at 30°C for 48 h. Colony counts were compared to those for no protein treatment controls to determine percentage viability.

For the time course assays, *Candida* at 5×10^4 CFU/ml (100 μl) was mixed with CCL28 variants at 2 μM (100 μl) in triplicates and then incubated for 1, 2, 4, 8, 10, 30, and 60 min at room temperature with gentle shaking. Amphotericin B (Thermo Fisher Scientific, Grand Island, NY) at 4 mg/ml was evaluated at the same time points as a control. For saturation assays, *Candida* suspensions of 2×10^7, 5×10^6, 5×10^5, and 5×10^4 CFU/ml (30 μl) were incubated with equal volumes of CCL28 variants at 1 μM in triplicates at room temperature for 2 h with gentle shaking. Plating and colony count enumeration were performed as described above.

Membrane disruption assays. *Candida* was cultured and washed as described above. Chemical killing was achieved by incubating *Candida* suspensions at 5×10^6 CFU/ml with equal volumes of a solution of 2% paraformaldehyde, 0.5% bovine serum albumin (BSA), and 2 mM EDTA in PBS at room temperature for 30 min. Cell death was confirmed by incubation on YPD plates for 48 h and colony enumeration. Chemically killed cells or live cells were washed twice and resuspended in PPB. Suspensions of killed or live *Candida* (100 μl) were incubated with equal volumes of PPB, paraformaldehyde solution, or the indicated CCL28 variant (0.25 μM unless otherwise specified) in triplicates for 10 min in 96-well plates. Cells were washed and resuspended with 1× PBS and then stained with propidium iodide (PI; Thermo Fisher Scientific, Grand Island, NY) at 1 mg/ml at room temperature in the dark for 10 min. Stained cells were washed with 1× PBS and resuspended in 200 μl of the paraformaldehyde solution. Cellular PI uptake was measured by flow cytometry in the CRI flow cytometry core on a BD LSR II (BD Biosciences, San Jose, CA, USA) and analyzed with FlowJo (Tree Star, Inc., Ashland, OR).

Adenylate kinase leakage was measured with an adenylate kinase assay (AKA) kit (Abcam, MA, USA). *Candida* cells at 2×10^7 CFU/ml in PPB (100 μl) and serial dilutions of indicated CCL28 variants (100 μl) were incubated for 10 min in triplicates in 96-well plates. Plates were centrifuged at 2,500 rpm for 3 min, and supernatant from each well (100 μl) was mixed with adenylate reagent (100 μl) in white 96-well flat-bottom assay plates. Luminescence was measured immediately by a SpectraMax plate reader (Molecular Devices, CA, USA).

Liposome preparation. The SUVs used for SAXS experiments were prepared as previously described (39, 68). Lyophilized phospholipids 1,2-dioleoyl-*sn*-glycero-3-phosphoethanolamine (DOPE), 1,2-dioleoyl-*sn*-glycero-3-phosphocholine (DOPC), and 1,2-dioleoyl-*sn*-glycero-3-phospho-L-serine (DOPS) from Avanti Polar Lipids were dissolved in chloroform to a concentration of 20 mg/ml as individual lipid stock solutions. Each lipid composition used to construct each model membrane was prepared by mixing the lipid stock solutions at the desired molar ratio. The produced lipid composition solutions were subsequently evaporated under nitrogen and desiccated overnight under vacuum. The resulting lipid film was resuspended in aqueous 140 mM NaCl, 10 mM HEPES (pH 7.4) to a concentration of 20 mg/ml and incubated overnight at 37°C. To form the SUVs, the lipid aqueous suspension was sonicated until clear and then extruded through a 0.2-μm-pore-size Anopore membrane filter (Whatman).

SAXS experiments with model membranes. SAXS experiments and data fitting were performed based on previously described protocols (37, 68–70). Lyophilized proteins (Δ3-CCL28 and Δ3-CCL28-Δ80) were solubilized in aqueous 140 mM NaCl, 10 mM HEPES (pH 7.4) and mixed with SUVs at P/L charge ratios of 1/4, 1/2, and 1/1. Samples were sealed in quartz capillaries (Mark-tubes; Hilgenberg GmbH) for SAXS measurements carried out at the Stanford Synchrotron Radiation Lightsource (SSRL; beamline 4-2) with monochromatic X rays at an energy of 9 keV. A DECTRIS PILATUS3 X 1M detector (172-μm pixel size) was used to collect the scattered radiation and the 2D SAXS powder patterns were integrated using the Nika 1.50 (71) package for Igor Pro 6.31 and FIT2D (72). Using Matlab software, the integrated scattering intensity $I(Q)$ was plotted against Q. Ratios of the measured peak positions ($Q_{measured}$) were compared with those of permitted reflections for different crystal phases to identify the phase(s) present in each sample. The lattice parameter, a, for each identified cubic phase is calculated using a linear regression through points corresponding to the peaks. For a cubic phase, $Q = (2\pi/a)\sqrt{h^2+k^2+l^2}$, where h, k, and l are Miller indices assigned to each peak. The slope of the linear fit ($m = 2\pi/a$) of $Q_{measured}$ versus $\sqrt{h^2+k^2+l^2}$ can be used to calculate a. The mean amount of Gaussian curvature, K, can be calculated using the equation $|<K>| = (2\pi\chi)/(A_0a^2)$, where the Euler characteristic, χ, and the surface area per unit

cell, A_0, are constants specific to each cubic phase, and a is the lattice parameter. For Ia3d, $\chi = -8$ and $A_0 = 3.091$; for Pn3m, $\chi = -2$ and $A_0 = 1.919$; for Im3m, $\chi = -4$ and $A_0 = 2.345$ (73).

Prediction of membrane active sequences in CCL28 using an SVM classifier. The CCL28 amino acid sequence (UniProt ID Q9NRJ3) was screened for AMP-like domains using a previously validated support vector machine (SVM) classifier trained to recognize membrane-permeating α-helical sequences (43). In brief, the SVM classifier outputs a σ-score for each input sequence, which corresponds to a probability that the sequence will induce NGC on a membrane, which is necessary for membrane permeation. A σ-score of greater than 1 corresponds to positive probability $P(+1)$ of >0.96. To assign a σ-score to each amino acid, we used a variable moving window along the full chemokine sequence and then averaged the scores for all the sequences in which each amino acid appeared. The resulting probability heat map was displayed onto the three-dimensional (3D) crystal structure of CCL28 (RCSB PDB 6CWS) in which the intensity values correspond to the mean σ-score, i.e., the probability that the amino acid is involved in inducing membrane permeability.

Statistical analysis. Analyses were performed using GraphPad Prism 8 (La Jolla, CA) or SPSS software version 24 (IBM Corp., Armonk, NY). Data were compared by Mann-Whitney or unpaired Student's *t* tests. A quadratic model for the weight loss over time was computed for each treatment group and across mouse sex. A mixed model was applied using time and intercept as random effects and mouse as clusters with an AR(1) covariance structure. IC_{50} curves were created for viability (percent) versus protein concentration. EC_{50} curves were created for PI uptake (percent) or luminescence versus protein concentration. Calculated *P* values of <0.05 were considered significant. All experiments were performed in duplicates at a minimum.

SUPPLEMENTAL MATERIAL

Supplemental material is available online only.

SUPPLEMENTAL FILE 1, PDF file, 0.4 MB.

ACKNOWLEDGMENTS

This work is supported in part by National Institutes of Health grants F30 HL134253 (M.A.T.), R01 AI052453 (M.W.L. and G.C.L.W.), R01 AI120655 (B.F.V.), and K08 DE026189 (A.R.H.). M.W.L. and G.C.L.W. are also supported by NSF DMR1808459 and the National Psoriasis Foundation. J.D.A. is supported by the NSF GRFP DGE-1650604. A.R.H. is also supported by the Children's Hospital of Wisconsin Research Institute and the Medical College of Wisconsin Department of Pediatrics. M.A.T. is a member of the NIH-supported (T32 GM080202) medical scientist training program at MCW.

Candida strains were kind gifts from Mira Edgerton (CAF4-2, Δ*dur3* Δ*dur31*) and Michail Lionakis (strains 24, 214, 216, 217, and 218). HPMC K100 premium LV gel was a gift from Colorcon Inc. We thank Ernest Lee for helpful discussions during the early stages of this work.

A.R.H., G.C.L.W., M.H.G., and B.F.V. conceived the project. J.H., M.A.T., J.D.A., M.W.L., and E.V.W. performed and analyzed all experiments. P.S. performed the statistical analysis. J.H., J.D.A., M.W.L., M.A.T., and A.R.H. wrote the original manuscript draft. J.H., M.A.T., P.S., G.C.L.W., M.H.G., B.F.V., and A.R.H. revised the manuscript. All authors reviewed the manuscript before submission.

B.F.V. has ownership interests in Protein Foundry, LLC.

REFERENCES

1. Brown GD, Denning DW, Gow NA, Levitz SM, Netea MG, White TC. 2012. Hidden killers: human fungal infections. Sci Transl Med 4:165rv13. https://doi.org/10.1126/scitranslmed.3004404.
2. Saiman L, Ludington E, Pfaller M, Rangel-Frausto S, Wiblin RT, Dawson J, Blumberg HM, Patterson JE, Rinaldi M, Edwards JE, Wenzel RP, Jarvis W. 2000. Risk factors for candidemia in neonatal intensive care unit patients. The National Epidemiology of Mycosis Survey study group. Pediatr Infect Dis J 19:319–324. https://doi.org/10.1097/00006454-200004000-00011.
3. Wey SB, Mori M, Pfaller MA, Woolson RF, Wenzel RP. 1989. Risk factors for hospital-acquired candidemia. A matched case-control study. Arch Intern Med 149:2349–2353. https://doi.org/10.1001/archinte.1989.00390100145030.
4. Kautzky S, Staudinger T, Presterl E. 2015. Invasive *Candida* infections in patients of a medical intensive care unit: attempt of improving diagnosis by quantifying the colonization. Wien Klin Wochenschr 127:132–142. https://doi.org/10.1007/s00508-014-0644-z.
5. Andes DR, Safdar N, Baddley JW, Playford G, Reboli AC, Rex JH, Sobel JD, Pappas PG, Kullberg BJ, Mycoses Study Group. 2012. Impact of treatment strategy on outcomes in patients with candidemia and other forms of invasive candidiasis: a patient-level quantitative review of randomized trials. Clin Infect Dis 54:1110–1122. https://doi.org/10.1093/cid/cis021.
6. Pfaller MA, Diekema DJ. 2007. Epidemiology of invasive candidiasis: a persistent public health problem. Clin Microbiol Rev 20:133–163. https://doi.org/10.1128/CMR.00029-06.
7. Novosad SA, Fike L, Dudeck MA, Allen-Bridson K, Edwards JR, Edens C, Sinkowitz-Cochran R, Powell K, Kuhar D. 2020. Pathogens causing central-line-associated bloodstream infections in acute-care hospitals-United States, 2011–2017. Infect Control Hosp Epidemiol 41:313–319. https://doi.org/10.1017/ice.2019.303.
8. Shao TY, Ang WXG, Jiang TT, Huang FS, Andersen H, Kinder JM, Pham G, Burg AR, Ruff B, Gonzalez T, Khurana Hershey GK, Haslam DB, Way SS. 2019. Commensal *Candida albicans* positively calibrates systemic Th17 immunological responses. Cell Host Microbe 25:404.e6–417.e6. https://doi.org/10.1016/j.chom.2019.02.004.
9. Moriyama B, Gordon LA, McCarthy M, Henning SA, Walsh TJ, Penzak SR.

2014. Emerging drugs and vaccines for candidemia. Mycoses 57:718–733. https://doi.org/10.1111/myc.12265.
10. Yang D, Biragyn A, Kwak LW, Oppenheim JJ. 2002. Mammalian defensins in immunity: more than just microbicidal. Trends Immunol 23:291–296. https://doi.org/10.1016/s1471-4906(02)02246-9.
11. Whibley N, Tritto E, Traggiai E, Kolbinger F, Moulin P, Brees D, Coleman BM, Mamo AJ, Garg AV, Jaycox JR, Siebenlist U, Kammuller M, Gaffen SL. 2016. Antibody blockade of IL-17 family cytokines in immunity to acute murine oral mucosal candidiasis. J Leukoc Biol 99:1153–1164. https://doi.org/10.1189/jlb.4A0915-428R.
12. Pan J, Kunkel EJ, Gosslar U, Lazarus N, Langdon P, Broadwell K, Vierra MA, Genovese MC, Butcher EC, Soler D. 2000. A novel chemokine ligand for CCR10 and CCR3 expressed by epithelial cells in mucosal tissues. J Immunol 165:2943–2949. https://doi.org/10.4049/jimmunol.165.6.2943.
13. Wang W, Soto H, Oldham ER, Buchanan ME, Homey B, Catron D, Jenkins N, Copeland NG, Gilbert DJ, Nguyen N, Abrams J, Kershenovich D, Smith K, McClanahan T, Vicari AP, Zlotnik A. 2000. Identification of a novel chemokine (CCL28), which binds CCR10 (GPR2). J Biol Chem 275:22313–22323. https://doi.org/10.1074/jbc.M001461200.
14. Hieshima K, Ohtani H, Shibano M, Izawa D, Nakayama T, Kawasaki Y, Shiba F, Shiota M, Katou F, Saito T, Yoshie O. 2003. CCL28 has dual roles in mucosal immunity as a chemokine with broad-spectrum antimicrobial activity. J Immunol 170:1452–1461. https://doi.org/10.4049/jimmunol.170.3.1452.
15. Lazarus NH, Kunkel EJ, Johnston B, Wilson E, Youngman KR, Butcher EC. 2003. A common mucosal chemokine (mucosae-associated epithelial chemokine/CCL28) selectively attracts IgA plasmablasts. J Immunol 170:3799–3805. https://doi.org/10.4049/jimmunol.170.7.3799.
16. Facciabene A, Peng X, Hagemann IS, Balint K, Barchetti A, Wang LP, Gimotty PA, Gilks CB, Lal P, Zhang L, Coukos G. 2011. Tumour hypoxia promotes tolerance and angiogenesis via CCL28 and T_{reg} cells. Nature 475:226–230. https://doi.org/10.1038/nature10169.
17. Nevins AM, Subramanian A, Tapia JL, Delgado DP, Tyler RC, Jensen DR, Ouellette AJ, Volkman BF. 2016. A requirement for metamorphic interconversion in the antimicrobial activity of chemokine XCL1. Biochemistry 55:3784–3793. https://doi.org/10.1021/acs.biochem.6b00353.
18. Watkins HR, Lapp CA, Hanes PJ, Dickinson DP, Volkmann KR, Newman CL, Konzelman JL. 2007. CCL28 effects on periodontal pathogens. J Periodontol 78:2356–2363. https://doi.org/10.1902/jop.2007.060504.
19. Jiang P, Lan J, Hu Y, Li D, Jiang G. 2012. Enhancing CCL28 expression through the gene transfer to salivary glands for controlling cariogenic microbe. Cytokine 59:94–99. https://doi.org/10.1016/j.cyto.2012.03.022.
20. Berri M, Virlogeux-Payant I, Chevaleyre C, Melo S, Zanello G, Salmon H, Meurens F. 2014. CCL28 involvement in mucosal tissues protection as a chemokine and as an antibacterial peptide. Dev Comp Immunol 44:286–290. https://doi.org/10.1016/j.dci.2014.01.005.
21. Sobirk SK, Morgelin M, Egesten A, Bates P, Shannon O, Collin M. 2013. Human chemokines as antimicrobial peptides with direct parasiticidal effect on *Leishmania mexicana in vitro*. PLoS One 8:e58129. https://doi.org/10.1371/journal.pone.0058129.
22. Thomas MA, He J, Peterson FC, Huppler AR, Volkman BF. 2018. The solution structure of CCL28 reveals structural lability that does not constrain antifungal activity. J Mol Biol 430:3266–3282. https://doi.org/10.1016/j.jmb.2018.06.001.
23. Thomas MA, Buelow BJ, Nevins AM, Jones SE, Peterson FC, Gundry RL, Grayson MH, Volkman BF. 2015. Structure-function analysis of CCL28 in the development of post-viral asthma. J Biol Chem 290:4528–4536. https://doi.org/10.1074/jbc.M114.627786.
24. Hernandez-Molina G, Burkhardt AM, Lima G, Zlotnik A, Betanzos JL, Bahena S, Llorente L. 2015. Absence of salivary CCL28 in primary Sjogren's syndrome. Rheumatol Int 35:1431–1434. https://doi.org/10.1007/s00296-014-3210-0.
25. Soto-Rojas AE, Villa AR, Sifuentes-Osornio J, Alarcon-Segovia D, Kraus A. 1998. Oral candidiasis and Sjogren's syndrome. J Rheumatol 25:911–915.
26. Yan Z, Young AL, Hua H, Xu Y. 2011. Multiple oral *Candida* infections in patients with Sjogren's syndrome – prevalence and clinical and drug susceptibility profiles. J Rheumatol 38:2428–2431. https://doi.org/10.3899/jrheum.100819.
27. UniProt Consortium T. 2018. UniProt: the universal protein knowledgebase. Nucleic Acids Res 46:2699. https://doi.org/10.1093/nar/gky092.
28. Kamai Y, Kubota M, Kamai Y, Hosokawa T, Fukuoka T, Filler SG. 2001. New model of oropharyngeal candidiasis in mice. Antimicrob Agents Chemother 45:3195–3197. https://doi.org/10.1128/AAC.45.11.3195-3197.2001.
29. Huppler AR, Conti HR, Hernandez-Santos N, Darville T, Biswas PS, Gaffen SL. 2014. Role of neutrophils in IL-17-dependent immunity to mucosal candidiasis. J Immunol 192:1745–1752. https://doi.org/10.4049/jimmunol.1302265.
30. Kong EF, Tsui C, Boyce H, Ibrahim A, Hoag SW, Karlsson AJ, Meiller TF, Jabra-Rizk MA. 2016. Development and *in vivo* evaluation of a novel histatin-5 bioadhesive hydrogel formulation against oral candidiasis. Antimicrob Agents Chemother 60:881–889. https://doi.org/10.1128/AAC.02624-15.
31. Shayeda GR, Palem CR, Rao YM. 2009. Development of novel bioadhesive buccal formulation of diltiazem: *in vitro* and *in vivo* characterization. PDA J Pharm Sci Technol 63:401–408.
32. Burdock GA. 2007. Safety assessment of hydroxypropyl methylcellulose as a food ingredient. Food Chem Toxicol 45:2341–2351. https://doi.org/10.1016/j.fct.2007.07.011.
33. Conti HR, Shen F, Nayyar N, Stocum E, Sun JN, Lindemann MJ, Ho AW, Hai JH, Yu JJ, Jung JW, Filler SG, Masso-Welch P, Edgerton M, Gaffen SL. 2009. Th17 cells and IL-17 receptor signaling are essential for mucosal host defense against oral candidiasis. J Exp Med 206:299–311. https://doi.org/10.1084/jem.20081463.
34. Huppler AR, Bishu S, Gaffen SL. 2012. Mucocutaneous candidiasis: the IL-17 pathway and implications for targeted immunotherapy. Arthritis Res Ther 14:217. https://doi.org/10.1186/ar3893.
35. Posteraro B, De Carolis E, Vella A, Sanguinetti M. 2013. MALDI-TOF mass spectrometry in the clinical mycology laboratory: identification of fungi and beyond. Expert Rev Proteomics 10:151–164. https://doi.org/10.1586/epr.13.8.
36. Kumar R, Chadha S, Saraswat D, Bajwa JS, Li RA, Conti HR, Edgerton M. 2011. Histatin 5 uptake by *Candida albicans* utilizes polyamine transporters Dur3 and Dur31 proteins. J Biol Chem 286:43748–43758. https://doi.org/10.1074/jbc.M111.311175.
37. Schmidt NW, Mishra A, Lai GH, Davis M, Sanders LK, Tran D, Garcia A, Tai KP, McCray PB, Ouellette AJ, Selsted ME, Wong GC. 2011. Criterion for amino acid composition of defensins and antimicrobial peptides based on geometry of membrane destabilization. J Am Chem Soc 133:6720–6727. https://doi.org/10.1021/ja200079a.
38. Schmidt NW, Mishra A, Wang J, DeGrado WF, Wong GC. 2013. Influenza virus A M2 protein generates negative Gaussian membrane curvature necessary for budding and scission. J Am Chem Soc 135:13710–13719. https://doi.org/10.1021/ja400146z.
39. Hu K, Schmidt NW, Zhu R, Jiang Y, Lai GH, Wei G, Palermo EF, Kuroda K, Wong GC, Yang L. 2013. A critical evaluation of random copolymer mimesis of homogeneous antimicrobial peptides. Macromolecules 46:1908–1915. https://doi.org/10.1021/ma302577e.
40. Schmidt NW, Deshayes S, Hawker S, Blacker A, Kasko AM, Wong GC. 2014. Engineering persister-specific antibiotics with synergistic antimicrobial functions. ACS Nano 8:8786–8793. https://doi.org/10.1021/nn502201a.
41. Yao H, Lee MW, Waring AJ, Wong GC, Hong M. 2015. Viral fusion protein transmembrane domain adopts beta-strand structure to facilitate membrane topological changes for virus-cell fusion. Proc Natl Acad Sci U S A 112:10926–10931. https://doi.org/10.1073/pnas.1501430112.
42. Lee MW, Lee EY, Lai GH, Kennedy NW, Posey AE, Xian W, Ferguson AL, Hill RB, Wong G. 2017. Molecular motor Dnm1 synergistically induces membrane curvature to facilitate mitochondrial fission. ACS Cent Sci 3:1156–1167. https://doi.org/10.1021/acscentsci.7b00338.
43. Lee EY, Fulan BM, Wong GC, Ferguson AL. 2016. Mapping membrane activity in undiscovered peptide sequence space using machine learning. Proc Natl Acad Sci U S A 113:13588–13593. https://doi.org/10.1073/pnas.1609893113.
44. Yount NY, Weaver DC, Lee EY, Lee MW, Wang H, Chan LC, Wong GCL, Yeaman MR. 2019. Unifying structural signature of eukaryotic alpha-helical host defense peptides. Proc Natl Acad Sci U S A 116:6944–6953. https://doi.org/10.1073/pnas.1819250116.
45. Edgerton M, Koshlukova SE, Lo TE, Chrzan BG, Straubinger RM, Raj PA. 1998. Candidacidal activity of salivary histatins. Identification of a histatin 5-binding protein on *Candida albicans*. J Biol Chem 273:20438–20447. https://doi.org/10.1074/jbc.273.32.20438.
46. Conti HR, Baker O, Freeman AF, Jang WS, Holland SM, Li RA, Edgerton M, Gaffen SL. 2011. New mechanism of oral immunity to mucosal candidiasis in hyper-IgE syndrome. Mucosal Immunol 4:448–455. https://doi.org/10.1038/mi.2011.5.
47. Kullberg BJ, van de Veerdonk F, Netea MG. 2014. Immunotherapy: a

potential adjunctive treatment for fungal infection. Curr Opin Infect Dis 27:511–516. https://doi.org/10.1097/QCO.0000000000000105.
48. Peters BM, Zhu J, Fidel PL, Jr, Scheper MA, Hackett W, El Shaye S, Jabra-Rizk MA. 2010. Protection of the oral mucosa by salivary histatin-5 against *Candida albicans* in an *ex vivo* murine model of oral infection. FEMS Yeast Res 10:597–604. https://doi.org/10.1111/j.1567-1364.2010.00632.x.
49. Matsuo K, Nagakubo D, Yamamoto S, Shigeta A, Tomida S, Fujita M, Hirata T, Tsunoda I, Nakayama T, Yoshie O. 2017. CCL28-deficient mice have reduced IgA antibody-secreting cells and an altered microbiota in the colon. J Immunol 200:800–809. https://doi.org/10.4049/jimmunol.1700037.
50. Burkhardt AM, Perez-Lopez A, Ushach I, Catalan-Dibene J, Nuccio SP, Chung LK, Hernandez-Ruiz M, Carnevale C, Raffatellu M, Zlotnik A. 2019. CCL28 Is involved in mucosal IgA responses, olfaction, and resistance to enteric infections. J Interferon Cytokine Res 39:214–223. https://doi.org/10.1089/jir.2018.0099.
51. Ghannoum MA, Rice LB. 1999. Antifungal agents: mode of action, mechanisms of resistance, and correlation of these mechanisms with bacterial resistance. Clin Microbiol Rev 12:501–517. https://doi.org/10.1128/CMR.12.4.501.
52. Raj PA, Edgerton M, Levine MJ. 1990. Salivary histatin 5: dependence of sequence, chain length, and helical conformation for candidacidal activity. J Biol Chem 265:3898–3905.
53. Jang WS, Bajwa JS, Sun JN, Edgerton M. 2010. Salivary histatin 5 internalization by translocation, but not endocytosis, is required for fungicidal activity in *Candida albicans*. Mol Microbiol 77:354–370. https://doi.org/10.1111/j.1365-2958.2010.07210.x.
54. Tati S, Li R, Puri S, Kumar R, Davidow P, Edgerton M. 2014. Histatin 5-spermidine conjugates have enhanced fungicidal activity and efficacy as a topical therapeutic for oral candidiasis. Antimicrob Agents Chemother 58:756–766. https://doi.org/10.1128/AAC.01851-13.
55. Liu B, Wilson E. 2010. The antimicrobial activity of CCL28 is dependent on C-terminal positively-charged amino acids. Eur J Immunol 40:186–196. https://doi.org/10.1002/eji.200939819.
56. Hernandez-Ruiz M, Zlotnik A. 2017. Mucosal Chemokines. J Interferon Cytokine Res 37:62–70. https://doi.org/10.1089/jir.2016.0076.
57. Ertugrul AS, Sahin H, Dikilitas A, Alpaslan N, Bozoglan A. 2013. Comparison of CCL28, interleukin-8, interleukin-1beta and tumor necrosis factor-alpha in subjects with gingivitis, chronic periodontitis and generalized aggressive periodontitis. J Periodontal Res 48:44–51. https://doi.org/10.1111/j.1600-0765.2012.01500.x.
58. Burkhardt AM, Tai KP, Flores-Guiterrez JP, Vilches-Cisneros N, Kamdar K, Barbosa-Quintana O, Valle-Rios R, Hevezi PA, Zuñiga J, Selman M, Ouellette AJ, Zlotnik A. 2012. CXCL17 is a mucosal chemokine elevated in idiopathic pulmonary fibrosis that exhibits broad antimicrobial activity. J Immunol 188:6399–6406. https://doi.org/10.4049/jimmunol.1102903.
59. Kakoei S, Hosseini B, Haghdoost AA, Sanjari M, Gholamhosseinian A, Afshar VF. 2015. Evaluation of salivary secretory immunoglobulin A levels in diabetic patients and association with oral and dental manifestations. Sultan Qaboos Univ Med J 15:e507–e511. https://doi.org/10.18295/squmj.2015.15.04.011.
60. Fukushima C, Matsuse H, Saeki S, Kawano T, Machida I, Kondo Y, Kohno S. 2005. Salivary IgA and oral candidiasis in asthmatic patients treated with inhaled corticosteroid. J Asthma 42:601–604. https://doi.org/10.1080/02770900500216259.
61. Prado GN, Suetomi K, Shumate D, Maxwell C, Ravindran A, Rajarathnam K, Navarro J. 2007. Chemokine signaling specificity: essential role for the N-terminal domain of chemokine receptors. Biochemistry 46:8961–8968. https://doi.org/10.1021/bi7004043.
62. Hoover DM, Boulegue C, Yang D, Oppenheim JJ, Tucker K, Lu W, Lubkowski J. 2002. The structure of human macrophage inflammatory protein-3alpha/CCL20. Linking antimicrobial and CC chemokine receptor-6-binding activities with human beta-defensins. J Biol Chem 277:37647–37654. https://doi.org/10.1074/jbc.M203907200.
63. Lin M, Carlson E, Diaconu E, Pearlman E. 2007. CXCL1/KC and CXCL5/LIX are selectively produced by corneal fibroblasts and mediate neutrophil infiltration to the corneal stroma in LPS keratitis. J Leukoc Biol 81:786–792. https://doi.org/10.1189/jlb.0806502.
64. Gahring LC, Osborne AV, Reed M, Rogers SW. 2010. Neuronal nicotinic alpha7 receptors modulate early neutrophil infiltration to sites of skin inflammation. J Neuroinflammation 7:38. https://doi.org/10.1186/1742-2094-7-38.
65. Menzies-Gow A, Ying S, Sabroe I, Stubbs VL, Soler D, Williams TJ, Kay AB. 2002. Eotaxin (CCL11) and eotaxin-2 (CCL24) induce recruitment of eosinophils, basophils, neutrophils, and macrophages as well as features of early- and late-phase allergic reactions following cutaneous injection in human atopic and nonatopic volunteers. J Immunol 169:2712–2718. https://doi.org/10.4049/jimmunol.169.5.2712.
66. Veldkamp CT, Peterson FC, Pelzek AJ, Volkman BF. 2005. The monomer-dimer equilibrium of stromal cell-derived factor-1 (CXCL 12) is altered by pH, phosphate, sulfate, and heparin. Protein Sci 14:1071–1081. https://doi.org/10.1110/ps.041219505.
67. Fonzi WA, Irwin MY. 1993. Isogenic strain construction and gene mapping in *Candida albicans*. Genetics 134:717–728.
68. Lee MW, Han M, Bossa GV, Snell C, Song Z, Tang H, Yin L, Cheng J, May S, Luijten E, Wong GC. 2017. Interactions between membranes and "metaphilic" polypeptide architectures with diverse side-chain populations. ACS Nano 11:2858–2871. https://doi.org/10.1021/acsnano.6b07981.
69. Xiong M, Lee MW, Mansbach RA, Song Z, Bao Y, Peek RM, Jr, Yao C, Chen LF, Ferguson AL, Wong GC, Cheng J. 2015. Helical antimicrobial polypeptides with radial amphiphilicity. Proc Natl Acad Sci U S A 112:13155–13160. https://doi.org/10.1073/pnas.1507893112.
70. Lande R, Lee EY, Palazzo R, Marinari B, Pietraforte I, Santos GS, Mattenberger Y, Spadaro F, Stefanantoni K, Iannace N, Dufour AM, Falchi M, Bianco M, Botti E, Bianchi L, Alvarez M, Riccieri V, Truchetet M-E, Wong GCL, Chizzolini C, Frasca L. 2019. CXCL4 assembles DNA into liquid crystalline complexes to amplify TLR9-mediated interferon-alpha production in systemic sclerosis. Nat Commun 10:1731. https://doi.org/10.1038/s41467-019-09683-z.
71. Ilavsky J. 2012. Nika: software for two-dimensional data reduction. J Appl Crystallogr 45:324–328. https://doi.org/10.1107/S0021889812004037.
72. Hammersley AP. 1997. FIT2D: an introduction and overview. ESRF97HA02T. European Synchrotron Radiation Facility, Grenoble, France.
73. Shearman GC, Ces O, Templer RH, Seddon JM. 2006. Inverse lyotropic phases of lipids and membrane curvature. J Phys Condens Matter 18:S1105–S1124. https://doi.org/10.1088/0953-8984/18/28/S01.